Entropy **2013**, *15*; 53-79; doi:10.3390/e15010053

OPEN ACCESS

entropy

ISSN 1099-4300

www.mdpi.com/journal/entropy

Article

Ordered Regions within a Nonlinear Time Series Solution of a Lorenz Form of the Townsend Equations for a Boundary-Layer Flow

LaVar King Isaacson

Professor Emeritus of Mechanical Engineering, University of Utah, 2067 Browning Avenue, Salt Lake City, UT 84108, USA; E-Mail: lkisaacson1@mac.com

Received: 21 August 2012; in revised form: 12 December 2012 / Accepted: 20 December 2012 / Published: 24 December 2012

Abstract: A modified form of the Townsend equations for the fluctuating velocity wave vectors is applied to a laminar three-dimensional boundary-layer flow. These equations are cast into a Lorenz-type system of equations. The initial system of Lorenz equations yields the generation of masked output signals containing internal ordered regions. The self-synchronizing property of the Lorenz system of equations is then exploited by considering the initial Lorenz system as a transmitter system providing chaotic masked information signals to a series of identical Lorenz receiver systems. The output signal from each successive receiver system indicates the growing recovery of ordered regions in the chaotic output signal. Finally, the three-dimensional graph of the output velocity wave vector signal from the fourth receiver system and the spectral entropy rates for the output axial velocity wave vector indicate the presence of ordered regions which are characterized as axially-directed spiral vortices.

Keywords: normal shock waves; boundary-layer flows; internal flow instabilities; spectral entropy rates; ordered regions; synchronized chaotic flow

PACS Codes: 47.40.Nm (Shock effects); 05.70.Ce (Entropy); 47.15.Fe (Stability of boundary-layers); 47.27.De (Ordered regions)

Nomenclature:

a_i	Fluctuating *i-th* component of velocity wave vector
b_1	Coefficient in modified Townsend equations defined by Equation (32)
f_r	Power spectral density of the fluctuating axial velocity wave vector
F	Time-dependent perturbation factor
j	Vertical station number in the boundary-layer computations
j	Time series data segment
k	Time-dependent wave number magnitude
k_i	Fluctuating *i-th* wave number of Fourier expansion
K	Adjustable weighting factor
M_1	Flight Mach number
M_2	Mach number downstream of a normal shock wave
nx	Axial station number in the boundary-layer computations
p	Hydrostatic pressure
p_1	Static pressure ahead of the normal shock wave
p_2	Static pressure behind the normal shock wave
P_r	Probability of the power spectral density of the *r-th* spectral segment
r_1	Coefficient in modified Townsend equations defined by Equation (30)
s_1	Coefficient in modified Townsend equations defined by Equation (31)
$s_{j\_}$	*spent* Spectral entropy rate over the j-th spectral segment
t	Time
t_1	Static temperature ahead of the normal shock wave
t_2	Static temperature behind the normal shock wave
T_{aw}	Adiabatic wall temperature
u	Axial boundary-layer velocity
u_e	Axial velocity at the outer edge of the x-y plane boundary layer
u_i	Fluctuating *i*-component of velocity instability
U_i	Mean velocity in the *i*-direction
v	Vertical boundary-layer velocity
V_y	Mean vertical velocity in the x-y plane
V_z	Mean vertical velocity in the z-y plane
w	Span wise boundary-layer velocity
w_e	Span wise velocity at the outer edge of the z-y plane boundary layer
W	Mean velocity in the span wise direction
x	Axial distance
x_i	*i-th* direction
x_j	*j-th* direction
y	Vertical distance
y_{xz}	Vertical distance to the x-z surface
z	Span wise distance

Greek Letters

δ_{lm}	Kronecker delta
η	Transformed vertical parameter
ν	Kinematic viscosity of the gas mixture
σ_{y1}	Coefficient in modified Townsend equations defined by Equation (28)
σ_{x1}	Coefficient in modified Townsend equations defined by Equation (29)

Subscripts

i, j, l, m	Tensor indices
r	The *r-th* index in the *j-th* time series data segment
x	Component in the x-direction
y	Component in the y-direction
z	Component in the z-direction

1. Introduction

Considerable progress has been made in understanding the physical processes associated with the process known as *bypass transition* and with the creation of so-called "exact coherent structures." Bypass transition is a transition process that may occur prior to the onset of regular instabilities leading to the transition from laminar to turbulent flow in wall-bounded shear layers. Berlin and Henningson [1] studied the receptivity of a laminar boundary layer to the imposition of simple vortical free-stream disturbances and found the production of streaks in the stream wise velocity component. Hoepffner and Brandt [2] presented a stochastic approach to the receptivity problem associated with the flow behavior in response to the presence of external disturbances of a chaotic nature. In this study, the streaks resulting from the nonlinear evolution of the optimal perturbations were found for Blasius boundary layer profiles.

Waleffe [3] found that traveling wave solutions of the Navier-Stokes equations for plane Couette and Poiseuille flows result from interactions of these streaky flows. These traveling waves were referred to in [3] as "exact coherent structures." Cherubini *et al*. [4] extended the analysis to Blasius boundary layer velocity profiles and found that these exact coherent structures exist on the "edge" between the laminar state and the turbulent state of the flow. Duguet *et al*. [5] studied the dynamics of the transition threshold in plane Couette flow subjected to certain types of localized initial disturbances and found that the "edge state" is an unsteady spot-like structure, which can be described as a dynamical system. Each of these five references contains bibliographies concerning both bypass transition and exact coherent structures.

The essential point for us here is to note than in all of these studies, the initial conditions for the study of the boundary layer behavior is the imposition of an external disturbance of some kind. The question may then be posed as to the possibility that initial disturbances may arise *internally* within the boundary layer, rather than imposed externally and then amplified within the boundary layer environment.

The objective of the research work reported in this article is to explore the possibility that instabilities may occur in laminar boundary layers over flat plate surfaces prior to normal transition

processes as a result of nonlinear interactions within the boundary layer itself, rather than being the result of disturbances imposed on the boundary layer from the external free stream.

The research is computational in nature, requiring appropriate mathematical models for each phase of the physical processes that may occur in the possible development of nonlinear instabilities within the laminar boundary layer environment

The flow stream developing a boundary layer flow over a flat surface is taken as a subsonic flow of an ideal gas, with negligible changes in temperature and density across the boundary layer profile. The usual assumption is made that the static pressure is constant across the boundary layer. Hence, the assumption of incompressibility is applicable and well-established computational procedures are employed to obtain the mean velocity gradients across the boundary layer profiles. The source code for the Keller-Cebeci Box method [6] has been implemented and serves as the computational procedure to obtain the numerical values for the velocity gradients across the boundary layers at various axial stations from the leading edge of the flat plate surface.

It has been found that a three-dimensional approach to the boundary layer velocity profiles is required for the prediction of instabilities within the boundary layer. This requirement is met by the inclusion of a flat-plate surface in the x-z plane of the flow configuration. Thus, similar Blasius velocity profiles (Hansen [7]) are obtained in both the x-y plane and in the z-y plane for inclusion as boundary conditions for the computation of any instability that may occur within the boundary layer environment.

The well-known Townsend equations (Townsend [8]) for the fluctuating velocity components occurring in a shear-flow environment are used as the starting point for the development of an appropriate model for the computation of instabilities due to nonlinear interactions within the boundary layer. These equations are Fourier transformed into a set of ordinary differential equations describing the time-dependent development of particular wave number vectors and a set of ordinary nonlinear differential equations describing the time-dependent development of the fluctuating velocity wave vectors.

The set of equations describing the time-development of the velocity wave vectors is then cast into a Lorenz-type format (Isaacson [9,10]). This format yields a low-dimensional deterministic set of equations that possess the characteristic of the prediction of chaotic solutions due to the inclusion of the nonlinear interaction terms within the equations. An internal feedback loop is included as a driver for the nonlinear transfer process between the axial fluctuating velocity wave vector and the vertical and span wise velocity wave vectors. This complete set of equations is termed the "modified Townsend equations."

These sets of time-dependent modified Townsend nonlinear equations are solved at specifically chosen vertical locations within the three-dimensional boundary-layer structure, with the previously computed boundary layer velocity gradients serving as input parameters for the solution of the modified Townsend equations.

The computational solution of the modified Townsend equations yields nonlinear time series for the three velocity wave vectors for the particular vertical location within the boundary layer. For selected values of kinematic viscosity and vertical location within the three-dimensional boundary layer structure, these nonlinear time series indicate the development of regions of rather short-term aperiodic instabilities.

Although only a limited number of oscillations appear in the time series (of the order of 6), the number of time steps included within this region is 4096. Burg's method (Chen [11], Press *et al*. [12]) is used to obtain the power spectral density for segments of limited data content over selected ranges of data within this selected time frame. Burg's method is particularly well suited for this process, as it has the property of isolating sharp peaks in the spectral data.

The concept of spectral entropy rate production (Powell and Percival [13]) is then used to characterize the oscillations as "chaotic", "partially-ordered", or "ordered" regions within the nonlinear time series output. When the spectral entropy rate production for a given segment goes to zero, we classify that region of the time series as "ordered."

In the field of communications, it has been found that the Lorenz system of nonlinear equations possesses the property of chaotic synchronization (Pecora and Carroll [14]), and that this synchronization could reveal ordered properties masked by chaotic components within the output signals (Perez and Cerdeiral [15], Cuomo and Oppenheim [16], Feng and Tse [17]). We decided to explore the concept that the initial nonlinear time series solution of the modified Townsend equations could perhaps be processed in place by additional sets of Lorenz-type equations. Following the nomenclature used in the communications field [16], we call the initial modified Townsend system a "transmitter" system, and each subsequent set of Lorenz-type equations a "receiver" system. The same set of boundary layer velocity profiles used for the transmitter system is used for each of the receiver systems. Again, from the communications field, the input to each of the receiver system of equations is the sum of the transmitter output of the axial fluctuating velocity wave signal plus the same (but reduced in value) outputs of the previous receiver systems. The results from this overall processing indicate a dramatic effect on the phase characteristics of the fluctuating velocity wave vector behavior. It is this processing that produces an axially directed spiral motion for the velocity wave vectors, which we have characterized as representing spiral vortices in the axial direction.

During the early phases of this research, it was found that the prediction of instabilities was very sensitive to the particular values for the kinematic viscosity for the boundary layer velocity gradients and for the initial conditions applied to the modified Townsend equations. It was also found that the subsonic conditions downstream of a normal shock wave at low supersonic speeds at the particular altitude of 21.3 km (Zucrow and Hoffman [18]) produced appropriate values of kinematic viscosity so that the mean velocity profiles within a subsonic laminar boundary layer over a flat plate would yield the prediction of the internal generation of instabilities within the boundary layer. The adiabatic wall temperatures produced by the relatively low subsonic flow conditions over the flat plate are sufficiently low as to allow the use of the incompressible boundary layer computational procedures discussed previously. With the use of an appropriate reference temperature, the incompressible form of the transformed boundary layer equations yields results very close to exact solutions.

To evaluate the considerable thermodynamic effects of normal shock waves, detailed partition functions (Sonntag and Van Wylen [19]) for each of the chosen gaseous species are evaluated at each set of temperature and pressure. The equilibrium chemical composition is determined for each set of temperature and pressure. The gas dynamic equations describing the normal shock wave [18] are iteratively solved, taking into account variable thermodynamic properties and variable chemical composition. The transport properties of each gaseous species (McBride *et al*. [20]) are evaluated at the downstream subsonic adiabatic wall temperature and static pressure. The Wilke approximation

(Dorrance [21]) is then used to compute the transport properties of the gas mixture. This process is iteratively solved until convergence is reached.

2. Supersonic Flow Environment

The flow configuration that we are approximating in this exploratory study is shown in Figure 1. The flow environment considered in this study is a flight Mach numbers of $M_1 = 1.44$ at an altitude of approximately 21.3 km. For these conditions, the atmospheric temperature is taken as $t_1 = 217.76$ K and the atmospheric pressure is $p_1 = 4.54 \times 10^3$ N/m^2 (Zucrow and Hoffman [22]).

Figure 1. Shown is a schematic diagram of the subsonic flow downstream of a normal shock wave. The x-y plane boundary-layer velocity profile is indicated.

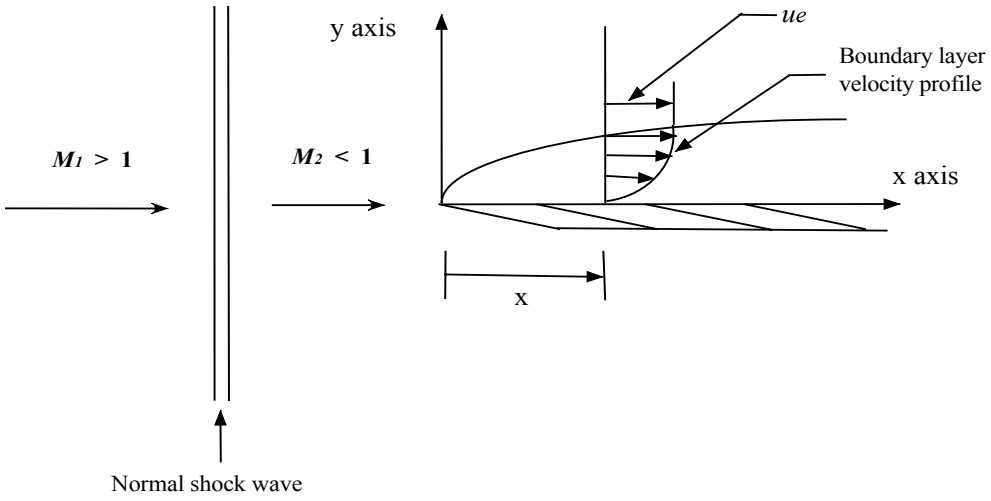

3. Thermo-Physical Properties

Thermodynamic and transport properties of high temperature air mixtures are required for the evaluation of the effects of the normal shock wave ahead of the flat plate on which the boundary-layer develops and for the determination of the adiabatic wall temperature that will be used to obtain the value of the kinematic viscosity. The mixture considered in this study is estimated from Figure 14.10 of Anderson [23]. This mixture consists of 0.934 percent argon (Ar), 0.00001 percent nitric oxide (NO), 20.95 percent oxygen (O_2), and 78.11 percent nitrogen (N_2), with percent by volume. The thermodynamic properties for this mixture as a function of temperature are obtained by the use of statistical thermodynamic partition functions [19]. The thermodynamic properties that are required for the calculation of the boundary-layer development are obtained from standard gas dynamic relations for normal shock waves [18]. The gas dynamic results are obtained assuming equilibrium thermodynamic properties and equilibrium chemical composition for the given gas mixture. The transport properties for each of the given gas species are obtained from [20]. The transport properties for mixtures of polyatomic gases are determined by the procedures presented in [21], including the Wilke approximation for mixtures of polyatomic gaseous species. The various thermodynamic and transport properties for the flight Mach number of $M_1 = 1.44$ at an altitude of 21.3 km are as follows:

Flight Mach number, M_1:	1.44	(1)
Ambient temperature, t_1:	217.88 K	(2)
Ambient static pressure, p_1:	4.524×10^3 N/m^2	(3)
Mach number, M_2:	0.72426	(4)
Static temperature, t_2:	279.135 K	(5)
Static pressure, p_2:	1.018×10^4 N/m^2	(6)
Adiabatic wall temperature, T_{aw}:	303.80 K	(7)
Mixture kinematic viscosity, ν:	1.602×10^{-4} m^2/s	(8)
Distance to x-z plane, y_{xz}:	0.00417	(9)

These properties are used for the computations in the transmitter systems and in each receiver system.

4. Computational Model for the Boundary-Layer Flow

The basic objective of this study is to use the boundary-layer flow environment computed with well-established computational tools to establish a basis for the determination of a set of spectral entropy rate values calculated at a specified location within the subsonic three dimensional laminar boundary-layer flow downstream of a given flight normal shock wave. A set of computer source codes developed for the computation of various wall shear environments has been presented in [6]. These source codes have been used to create computer programs required to compute the desired boundary-layer flow, including the necessary gradients in the mean velocities in a three-dimensional configuration.

The flow configuration we wish to model is the three-dimensional wall shear layer downstream of an initial starting plane, as indicated in Figure 2. The label on the center right side of the schematic indicates a flat plate surface placed at a height y in the x-z plane with the leading edge in the negative x-z plane and the trailing edge along the x-y plane. A span wise velocity of w_e, has been included in the overall flow configuration. The surface and the cross-flow velocity have been added to provide the appropriate similar Blasius boundary layer velocity profile in the z-y plane. The overall flow is thus three-dimensional with both axial and span wise velocity components. The x-y boundary-layer velocity profile is shown in Figure 1.

Figure 2. The three-dimensional flow model and the coordinate system for the boundary layer flow environment. Note the y-location for the z-y plane flat plate boundary-layer velocity profile.

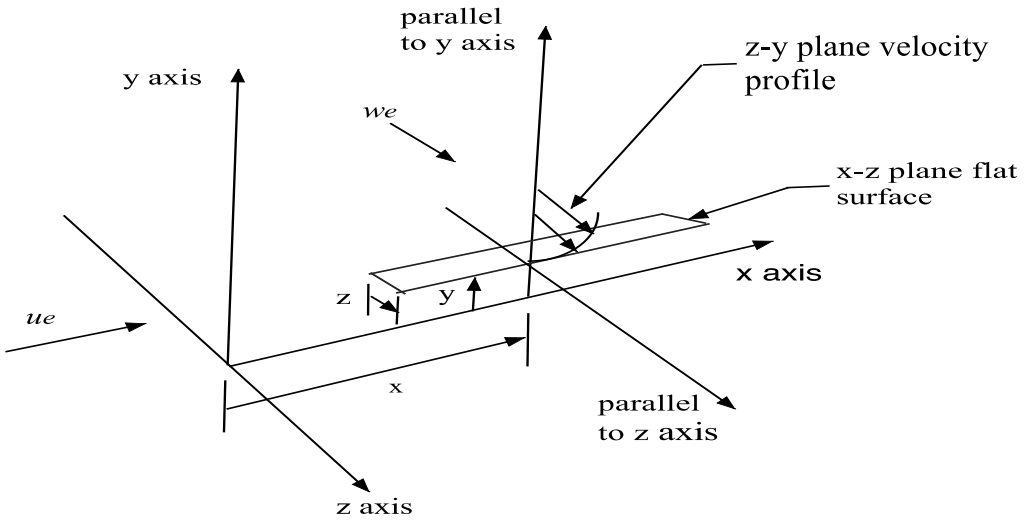

The computational procedure developed in [6] is used as the basis for our computations of the three-dimensional boundary-layer flow. The flow is of the Blasius type with zero pressure gradients in both the axial and span wise directions. The modification, which we introduce, is to impose an initial free stream velocity of unity, making the boundary-layer edge velocity dimensionless. The main computer program in the computational procedure developed in [6] establishes "*nx*" as the station number for the axial direction and the symbol "*j*" for the vertical grid number for the calculation of the vertical profiles at a given axial or span wise station. We will also include the corresponding axial distance with the *nx* value and the corresponding η value with the vertical station number *j*.

In an analysis of the conditions for similarity in boundary-layer flows, Hansen [7] indicates that the Blasius profile of the velocity gradient in the x-y plane and the Blasius profile in the z-y plane along the original starting planes are similar. Hence, we apply the computer methods of [6] to the computation of the laminar velocity profile in the x-y plane at the axial station, $nx = 4$ (x = 0.08), along the x-axis, and the same computer methods to the computation of the laminar velocity profile in the z-y plane at the span wise station, $nz = 4$ (z = 0.003), along the z-axis, with no pressure gradient in the z direction. The x-z surface for the development of the z-y plane boundary layer is raised an appropriate distance, y_{xz}, from the x-z plane to bring the transformed z-y boundary-layer velocity gradients into line with the transformed x-y boundary-layer velocity gradients.

The velocity gradients in both the x-y plane and the z-y plane are required for the evaluation of instabilities produced within the boundary-layer flow. These values thus form a set of strain rate parameters required for the internal transfer of kinetic energy from the mean flow into the fluctuating velocity components.

The velocity profiles are obtained from the computational procedure at $nx = 4$ (x = 0.08), thus initially computing the boundary layer as laminar. The length and width of the primary flat plate are each taken as 1.0 m.

For the flow in the z direction, we take the external velocity $w_e = 0.10$, with a pressure gradient of zero in the z direction. The z-y plane laminar velocity gradients are obtained at a span wise station of $nz = 4$ (z = 0.003), at the axial station of $nx = 4$ (x = 0.08), with the x-z plane flat plate surface at a height of y_{xz}. This procedure brings the location of the transformed z-y boundary-layer velocity gradients into alignment with the transformed x-y boundary-layer velocity gradients for the evaluation of the modified Townsend equations for the boundary-layer instabilities.

5. Mathematical Model of the Flow Instability

5.1. Transformation of the Townsend Equations

The Navier-Stokes equations describing this flow are transformed through a Fourier analysis into a Lorenz-type format, specifically keeping the nonlinear coupling terms. Using the Fourier expansion procedure as presented by Townsend [8], the equations of motion for the boundary-layer flow may be separated into steady plus fluctuating values of the velocity components. The velocity fluctuations around the mean values of the velocity components will thus be of primary interest. The equations for the velocity fluctuations may be written as follows:

$$\frac{\partial u_i}{\partial t} + U_i \frac{\partial u_i}{\partial x_j} + u_i \frac{\partial U_i}{\partial x_j} + u_i \frac{\partial u_i}{\partial x_j} = -\frac{\partial p}{\partial x_i} + \nu \frac{\partial^2 u_i}{\partial x_j^{\,2}} \tag{10}$$

In these equations, ν is the kinematic viscosity. The pressure term may be transformed as:

$$-\frac{\partial^2 p}{\partial x_l^{\,2}} = 2\frac{\partial U_l}{\partial x_m}\frac{\partial u_m}{\partial x_l} + \frac{\partial u_l}{\partial x_m}\frac{\partial u_m}{\partial x_l}. \tag{11}$$

In these expressions, the mean velocity components are denoted by U_i, with i = 1,2,3 representing the x, y, and z components, while x_j, with j = 1,2,3 denote the x, y and z directions. The three mean velocity components and the nine gradients in the mean velocities are obtained from the solutions for the boundary layer flows as outlined in [6].

As pointed out in [8], the pressure is determined by the velocity and temperature fields and is not a local quantity but depends on the entire field of velocity and temperature. The elimination of the pressure fluctuation term introduces nonlinear coupling between the velocity coefficients. In our work here, we will introduce an internal feedback mechanism that will model the nonlinear interaction process but will allow the resulting equations to be integrated in time. The velocity fluctuations may be expanded in terms of a sum of Fourier components as:

$$u_i(x) = \sum a_i(k) \exp(ik \cdot x). \tag{12}$$

The variation with time of each Fourier component of the fluctuation field is then given by the equation for each of the velocity wave vector amplitudes:

$$\begin{aligned} \frac{da_i(k)}{dt} &= -\nu k^2 a_i(k) - \frac{\partial U_i}{\partial x_i} a_i(k) + 2\frac{k_i k_l}{k^2}\frac{\partial U_l}{\partial x_m} a_i(k) \\ &+ i \sum_{k'+k''=k} (k_l \frac{k_l k_m}{k^2} - \delta_{im} k_l) a_l(k') a_m(k''). \end{aligned} \tag{13}$$

The equations for the rate of change of the wave numbers are:

$$\frac{dk_i}{dt} = -\frac{\partial U_l}{\partial x_i} k_l. \tag{14}$$

Sagaut and Cambon [24] and Mathieu and Scott [25] have characterized the coefficients of the nonlinear velocity products in the fourth term on the right-hand side of Equation (14):

$$(\delta_{im} - \frac{k_l k_m}{k^2}), \tag{15}$$

as a projection matrix, projecting any given velocity wave vector, a_i, perpendicular to the direction of the corresponding wave number, k_i. These authors interpret this matrix as a transfer operator for the transfer of kinetic energy occurring at low wavenumber modes, as a 'pumping' mechanism, toward higher wavenumber modes by nonlinear interactions.

We wish to close the set of equations, Equation (13), by replacing the projection matrix with an appropriate model equation that accomplishes the transfer process. To get an approximate form for the coefficient of the nonlinear transfer coefficient, results from perturbation theory provide a convenient model equation that has proven to be quite useful. Landau and Lifshitz [26] give an expression developed by quantum mechanics perturbation theory for the probability of a transition of a quantum

system from a state m to state n under the influence of a periodic perturbation. This expression involves a coefficient of the form (1 – cos (f (t)), (where f (t) is a function of the time t), in the probability function for finding the system in the new state n at time t. We have heuristically adopted this format for our model transfer equation. Pyragas [27] gives a specific form for such an internal feedback control signal that involves a weighting factor and an internally generated disturbance signal. We have combined these elements is such a manner so that the projection matrix in Equation (13) is replaced by the expression:

$$(1 - K^{\perp} \cos(\, k(t)\,)) \tag{16}$$

K is a small, adjustable weighting factor [27] and $k(t)$ is the magnitude of the time-dependent axial wave number vector given by:

$$k(t) = \sqrt{(k_x^2)}\,. \tag{17}$$

To simplify the nomenclature, we define F as:

$$F = K^{\perp} \cos(\, k(t)\,). \tag{18}$$

The three deterministic equations for the velocity wave vectors may then be written as:

$$\begin{aligned} \frac{da_x}{dt} &= \left[\left(\frac{2k_xk_x}{k^2} - 1\right)\frac{\partial U}{\partial y} + \frac{2k_xk_y}{k^2}\frac{\partial V_x}{\partial y} + \frac{2k_xk_z}{k^2}\frac{\partial W}{\partial y}\right]a_y \\ &- \left\{\nu k^2 - \left[\left(\frac{2k_xk_x}{k^2} - 1\right)\frac{\partial U}{\partial x} + \frac{2k_xk_y}{k^2}\frac{\partial V_x}{\partial x} + \frac{2k_xk_z}{k^2}\frac{\partial W}{\partial x}\right]\right\}a_x \end{aligned} \tag{19}$$

$$\begin{aligned} \frac{da_y}{dt} &= -(1-F)a_xa_z + \left[\frac{2k_yk_x}{k^2}\frac{\partial U}{\partial x} + \left(\frac{2k_yk_y}{k^2} - 1\right)\frac{\partial V_x}{\partial x} + \frac{2k_yk_z}{k^2}\frac{\partial W}{\partial x}\right]a_x \\ &- \left\{\nu k^2 - \left[\frac{2k_yk_x}{k^2}\frac{\partial U}{\partial y} + \left(\frac{2k_yk_y}{k^2} - 1\right)\frac{\partial V_z}{\partial y} + \frac{2k_yk_z}{k^2}\frac{\partial W}{\partial y}\right]\right\}a_y \end{aligned} \tag{20}$$

$$\frac{da_z}{dt} = (1-F)a_xa_y - \left\{\nu k^2 - \left[\frac{2k_zk_x}{k^2}\frac{\partial U}{\partial z} + \frac{2k_zk_y}{k^2}\frac{\partial V_z}{\partial z} + \left(\frac{2k_zk_z}{k^2} - 1\right)\frac{\partial W}{\partial z}\right]\right\}a_z \tag{21}$$

Note that the internal feedback factor $(1-F)$ is applied to the nonlinear terms in the equations for $\frac{da_y}{dt}$ and $\frac{da_z}{dt}$, and not to one of the directly accessible dependent variables. The application of the perturbation factor in this fashion implies that the nonlinear terms in the first-order equations for the velocity wave vector fluctuations represent a 'pumping' process, transferring energy from the axial velocity wave vector, a_x, into the vertical velocity wave vector, a_y, and the span wise velocity wave vector, a_z.

The set of equations for the time-dependent wave numbers is obtained by including the gradients of the mean velocities in the x-y and z-y boundary layers as follows:

$$\frac{dk_x}{dt} = -\frac{\partial U}{\partial x}k_x - \frac{\partial V_x}{\partial x}k_y \tag{22}$$

$$\frac{dk_y}{dt} = -\frac{\partial U}{\partial y}k_x - \frac{\partial V_x}{\partial y}k_y - \frac{\partial W}{\partial y}k_z \tag{23}$$

$$\frac{dk_z}{dt} = -\frac{\partial V_z}{\partial z}k_y - \frac{\partial W}{\partial z}k_z . \tag{24}$$

With these approximations, we uncouple the continuity equations for the wave numbers from the solutions of the nonlinear deterministic equations for the velocity fluctuation wave vectors. The equations for the fluctuating velocity components have thus been transformed into a form similar to Lorenz-type equations, as shown by Hellberg and Orszag [28] and Isaacson [29]. The values of the mean velocity gradients as determined in the solution of the boundary-layer flows and a weighting factor accounting for the degree of internal feedback included in the nonlinear coupling terms in the modified Townsend equations are the only parameters required for the solution of the resulting set of six simultaneous equations describing the possible generation of instabilities within the boundary-layer environment.

The theoretical modeling of the internal flow instabilities within the boundary-layer flow consists of six simultaneous first-order differential equations, solved at the vertical station of j = 16 within the wall shear layer. The solution of the set of equations describing the flow instabilities yields the velocity-fluctuation wave-vectors in three-dimensions for this particular vertical station at the axial station of nx = 4 (x = 0.08) and the span wise station of nz = 4 (z = 0.003) and the value of the vertical location y_{xz} = 0.00417 of the z-y plane boundary-layer surface.

The equations are integrated using a fourth-order Runge-Kutta technique with computer source codes as presented by Press *et al.* [30]. First, the three first-order differential equations for the wave numbers are integrated in time with the resulting series stored to files on the hard drive. A time step of 0.0001 s is used with a total of 12,288 time steps included in the integration process. These stored data files thus become available for the solution of the time-dependent deterministic equations for the fluctuating velocity wave vectors. The resulting axial velocity wave vector nonlinear time series signal is then processed to characterize the signal within the various regions and to compute the spectral entropy rates within those regions.

Figure 3 presents the resulting time dependent perturbation factor, F, as a function of time step over the complete computation range. It should be noted that this factor is a continuously varying parameter throughout the computations of the boundary-layer instabilities.

Figure 4 presents the variation of the fluctuating axial velocity wave vector as a function of the time step. These results indicate that after a period of induction, oscillatory instabilities develop in the fluctuating axial velocity wave vector.

Figure 5 presents the phase diagram of the fluctuating vertical velocity wave vector as a function of the fluctuating axial velocity wave for the selected range of time step values. Two separate regions are indicated. The first, inner region indicates a Lorenz-type behavior, while the second region indicates a rather uniform oscillation of the velocity wave vectors.

Figure 3. The time dependent internal feedback parameter, F, for the initial Lorenz system is shown as a function of the time step. Parameters: $M_1 = 1.44$, $\xi = 0.08$, $\zeta = 0.003$, $j = 16$ ($\eta = 3.00$).

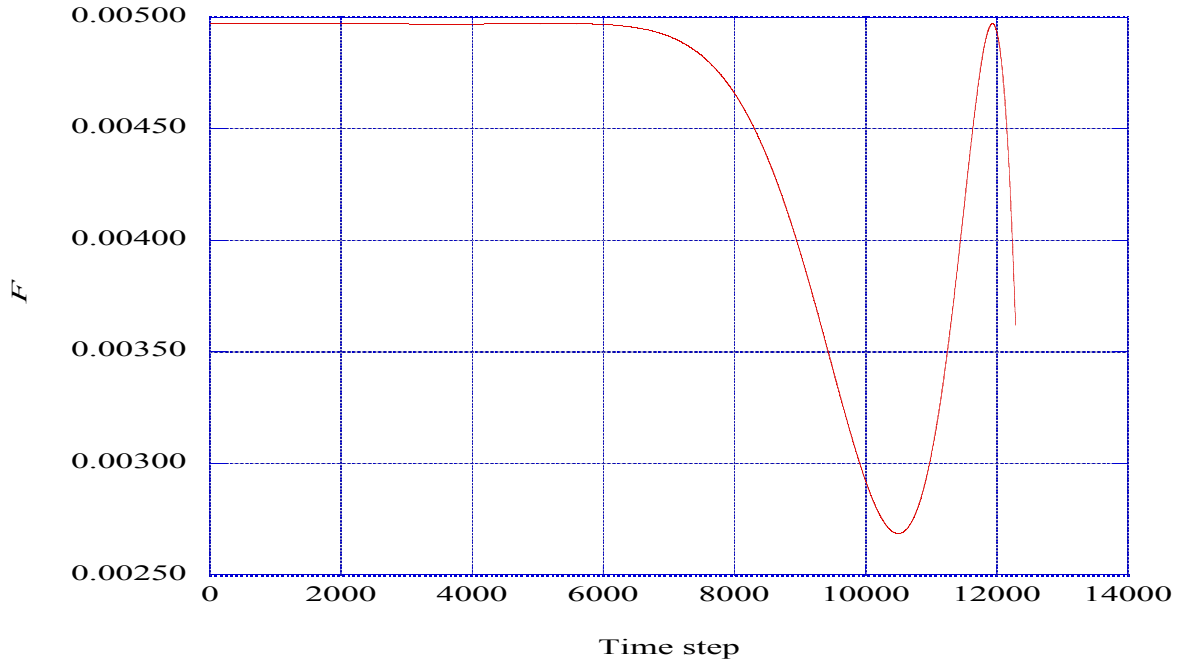

Figure 4. The axial velocity wave vector output, a_{x1} from the initial Lorenz system is shown as a function of the time step. Parameters: $M_1 = 1.44$, $x = 0.08$, $z = 0.003$, $j = 16$ ($\eta = 3.00$).

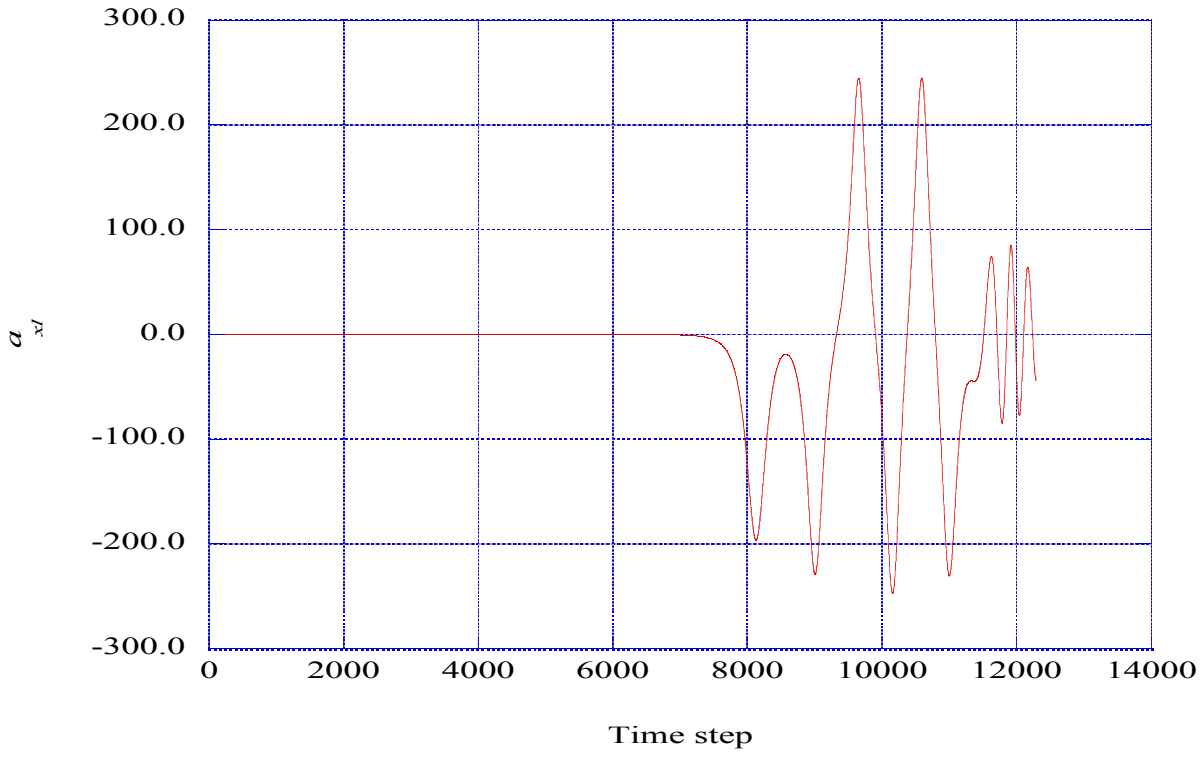

Figure 5. The phase plane, $a_{x1} - a_{y1}$ for the output of the initial Lorenz system is shown. Parameters: $M_1 = 1.44$, $x = 0.08$, $z = 0.003$, $j = 16$ ($\eta = 3.00$).

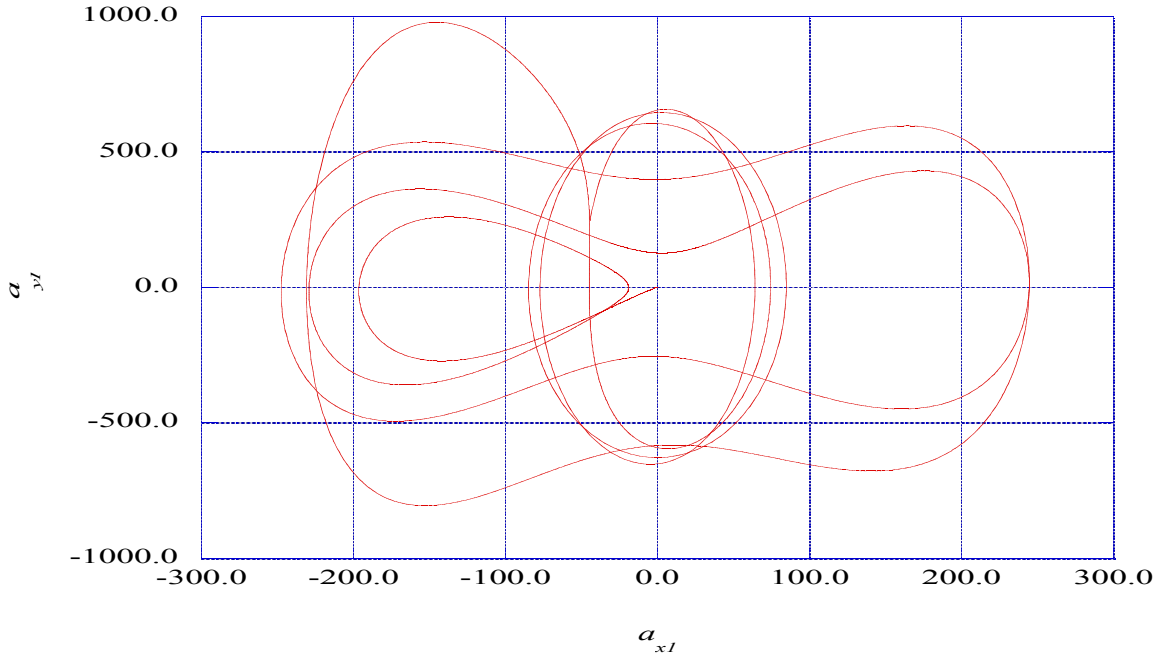

Figure 6 shows the phase diagram for the $a_{z1} - a_{y1}$ output signals from the initial Lorenz system, the transmitter system. An aperiodic oscillating system is shown in the initial period of the time segment with the more periodic oscillations moving in the negative span wise direction in the latter portions of the integration time period. The $a_{z1} - a_{y1}$ phase plane output signals from this initial system will be transformed by the subsequent receiver systems, as described in the next section, into the opposite direction, with the more periodic motion moving in the positive span wise direction.

Figure 6. The phase plane, $a_{z1} - a_{y1}$ for the output of the initial Lorenz system is shown. Parameters: $M_1 = 1.44$, $x = 0.08$, $z = 0.003$, $y_{xz} = 0.00417$, $j = 16$ ($\eta = 3.00$).

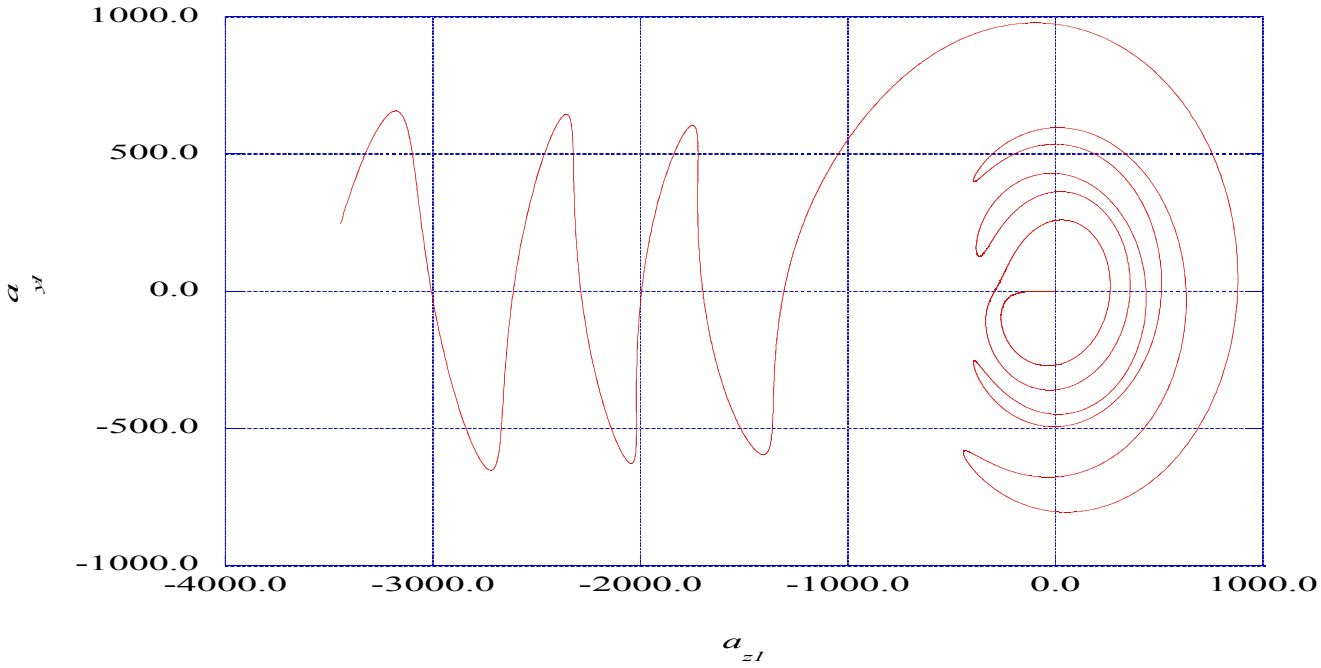

Figure 7 shows the three-dimensional representation of the fluctuating velocity wave vectors produced by the transmitter system. This result indicates a close similarity with a three-dimensional representation of the original Lorenz system of equations. However, the region of Lorenz-like aperiodicity and the region of nearly periodic behavior of the trajectories are apparent.

Figure 7. The three-dimensional representation of the fluctuating velocity wave vector trajectories produced by the initial Lorenz system is shown. Parameters: M_1 = 1.44, x = 0.08, z = 0.003, j = 16 (η = 3.00).

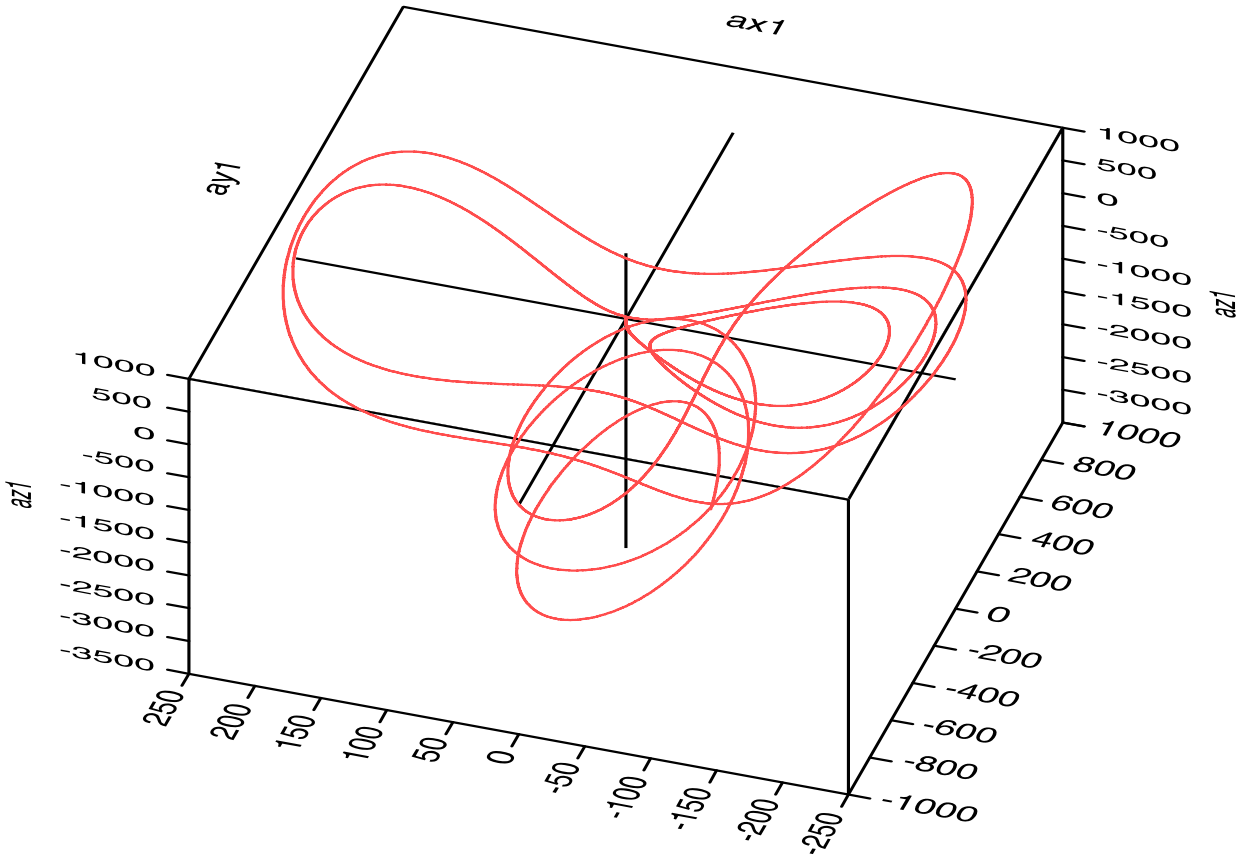

The effects of the synchronization of the chaotic output signals by the subsequent Lorenz-like receiver systems will become apparent through the representation of each receiver output signal in a three-dimensional presentation.

5.2. Extracting Ordered Signals from Nonlinear Instability Time Series

Perez and Cerdeiral [15] and Cuomo and Oppenheim [16] present methods for extracting messages that are masked by chaotic signals. Feng and Tse [17] have recently reviewed the various approaches used for the reconstruction of chaotic signals as applied in chaos-based communications. Reference [17] also presents an extensive bibliography of recent work in the application of chaos theory in the field of chaos-based communications. The method of extracting information from messages that are masked by chaotic signals is adapted here to extract ordered signals from the chaotic output of the modified Townsend equations describing the instabilities occurring in a particular laminar boundary layer flow.

The modified Townsend equations discussed in the previous section have been caste into a Lorenz form, which we now consider as an initial transmitter system for a series of in place identical Lorenz receiver systems. We use the approach from communications theory based on signal masking occurring in the transmitter system, and signal recovery in the subsequent receiver systems.

We consider the initial Lorenz system as the transmitter. The various coefficients in each of the receiver systems are computed in the same manner as in the transmitter system. Following the results in [14], the output for the axial velocity wave vector from the transmitter is used as input to the first receiver system. The input to the next receiver system is then made up of the sum of the output from the transmitter system plus the output from the first receiver system. This process is repeated over four receiver systems until the ordered information is recovered.

The modified Townsend equations are written for the transmitter system in the following abbreviated form:

$$\frac{da_{x1}}{dt} = \sigma_{y1} a_{y1} - \sigma_{x1} a_{x1} \tag{25}$$

$$\frac{da_{y1}}{dt} = -(1-F) a_{x1} a_{z1} + r_1 a_{x1} - s_1 a_{y1} \tag{26}$$

$$\frac{da_{z1}}{dt} = (1-F) a_{x1} a_{y1} - b_1 a_{z1} \tag{27}$$

In these equations, the respective time-dependent coefficients have the following forms:

$$\sigma_{y1} = \left[\left(\frac{2k_x k_x}{k^2} - 1 \right) \frac{\partial U}{\partial y} + \frac{2k_x k_y}{k^2} \frac{\partial V_x}{\partial y} + \frac{2k_x k_z}{k^2} \frac{\partial W}{\partial y} \right] \tag{28}$$

$$\sigma_{x1} = \left\{ \nu k^2 - \left[\left(\frac{2k_x k_x}{k^2} - 1 \right) \frac{\partial U}{\partial x} + \frac{2k_x k_y}{k^2} \frac{\partial V_x}{\partial x} + \frac{2k_x k_z}{k^2} \frac{\partial W}{\partial x} \right] \right\} \tag{29}$$

$$r_1 = \left[\frac{2k_y k_x}{k^2} \frac{\partial U}{\partial x} + \left(\frac{2k_y k_y}{k^2} - 1 \right) \frac{\partial V_x}{\partial x} + \frac{2k_y k_z}{k^2} \frac{\partial W}{\partial x} \right] \tag{30}$$

$$s_1 = \left\{ \nu k^2 - \left[\frac{2k_y k_x}{k^2} \frac{\partial U}{\partial y} + \left(\frac{2k_y k_y}{k^2} - 1 \right) \frac{\partial V_z}{\partial y} + \frac{2k_y k_z}{k^2} \frac{\partial W}{\partial y} \right] \right\} \tag{31}$$

$$b_1 = \left\{ \nu k^2 - \left[\frac{2k_z k_x}{k^2} \frac{\partial U}{\partial z} + \frac{2k_z k_y}{k^2} \frac{\partial V_z}{\partial z} + \left(\frac{2k_z k_z}{k^2} - 1 \right) \frac{\partial W}{\partial z} \right] \right\} \tag{32}$$

For the nth receiver system, the system of dynamic equations is written as:

$$\frac{da_{xn}}{dt} = \sigma_{y1} a_{yn} - \sigma_{x1} a_{xn} \tag{33}$$

$$\frac{da_{yn}}{dt} = -a_{rn} a_{zn} + r_1 a_{xn} - s_1 a_{yn} \tag{34}$$

$$\frac{da_{zn}}{dt} = a_{rn} a_{yn} - b_1 a_{zn} \tag{35}$$

In these expressions, the input signal carrying the information from the transmitter and the previous receivers to the rth receiver is given by:

$$a_{rn} = \sum_{i=1}^{i=n-1} a_{xi} \qquad (\text{n} >= 2) \tag{36}$$

The time-dependent input for the first receiver consists of the output of the initial transmitter system, a_{x1}. The initial value for the fluctuating axial velocity wave vector for the transmitter system is equal to 0.200, while the initial value for the corresponding variable for each successive receiver system is set equal to 0.100 Lower initial values for the receiver systems result in much lower levels for the output signal of each of the receiver systems. This process determines the result that the outputs from each of the receiver systems will be masked by the original transmitter output signal, and that the synchronization process will yield an indication of any ordered regions within the transmitter signal.

The input for the second receiver is the sum of the output a_{x1} from the initial transmitter and the output from the first receiver, a_{x2}. This summation process is repeated for the input signal to each subsequent receiver.

Figure 8 shows the $a_{x2} - a_{y2}$ phase plane results obtained from the output of the first receiver. Figure 9 shows the $a_{z2} - a_{y2}$ phase plane results for this receiver. The processing of the input signal by the receiver system has resulted in a shifting of the orientation of the phase plane results for both sets of results from that indicated for the transmitter system.

Figure 8. This figure presents the phase plane, $a_{x2} - a_{y2}$ for the output of the first receiver system. Parameters: $M_1 = 1.44$, $x = 0.08$, $z = 0.003$, $j = 16$ ($\eta = 3.00$).

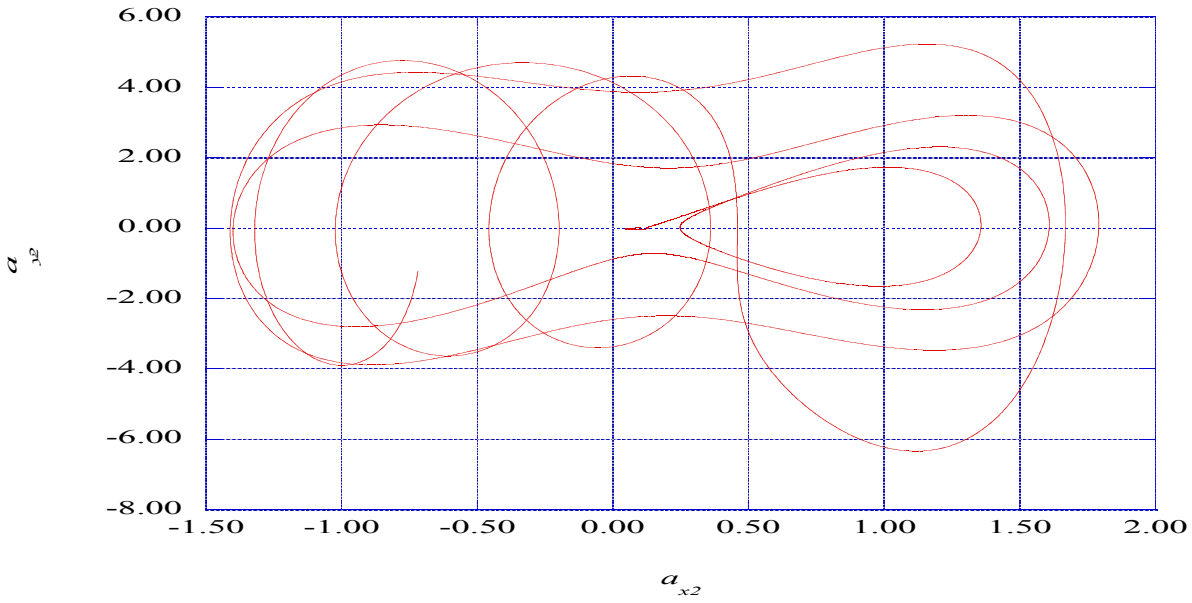

Figure 10 presents the three-dimensional plot of the output for the three velocity wave vectors from the first receiver system. It is interesting to note that the first receiver has begun to reorient the velocity wave vectors, and that the emergence of an ordered structure in the a_x and a_y velocity wave vectors is apparent.

Figure 9. This figure presents the phase plane, $a_{z2} - a_{y2}$ for the output of the first receiver system. Parameters: $M_1 = 1.44$, $x = 0.08$, $z = 0.003$, $j = 16$ ($\eta = 3.00$).

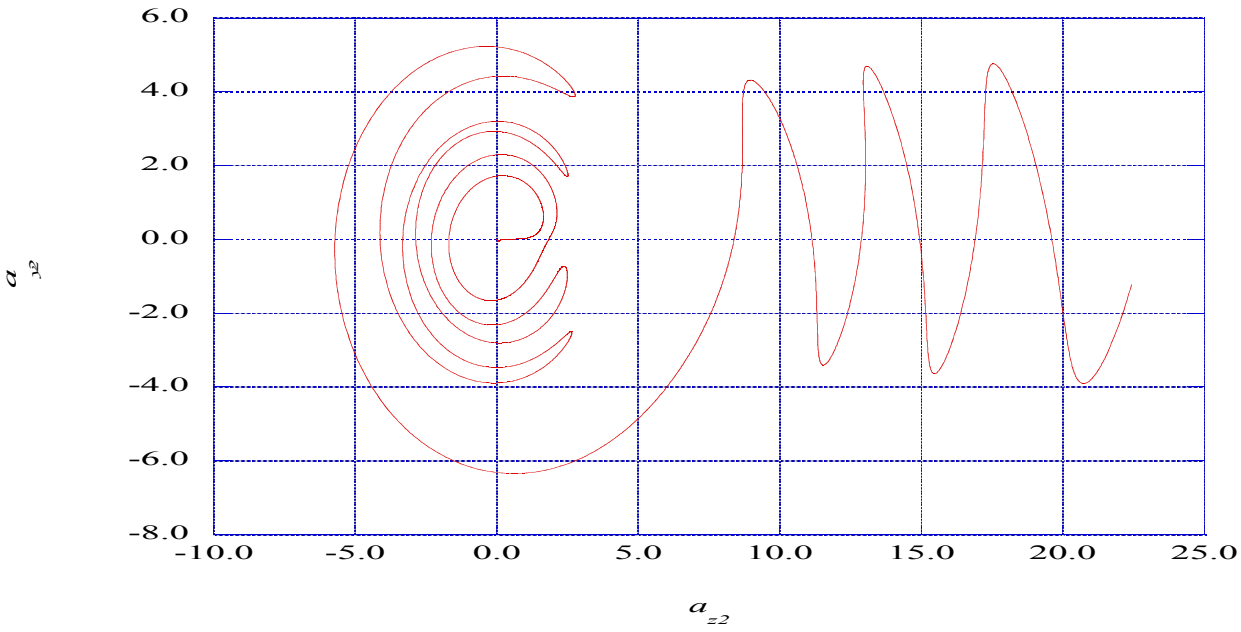

Figure 10. This figure presents a three-dimensional representation of the fluctuating velocity wave vector trajectories produced through the first receiver system. Parameters: $M_1 = 1.44$, $x = 0.08$, $z = 0.003$, $j = 16$ ($\eta = 3.00$).

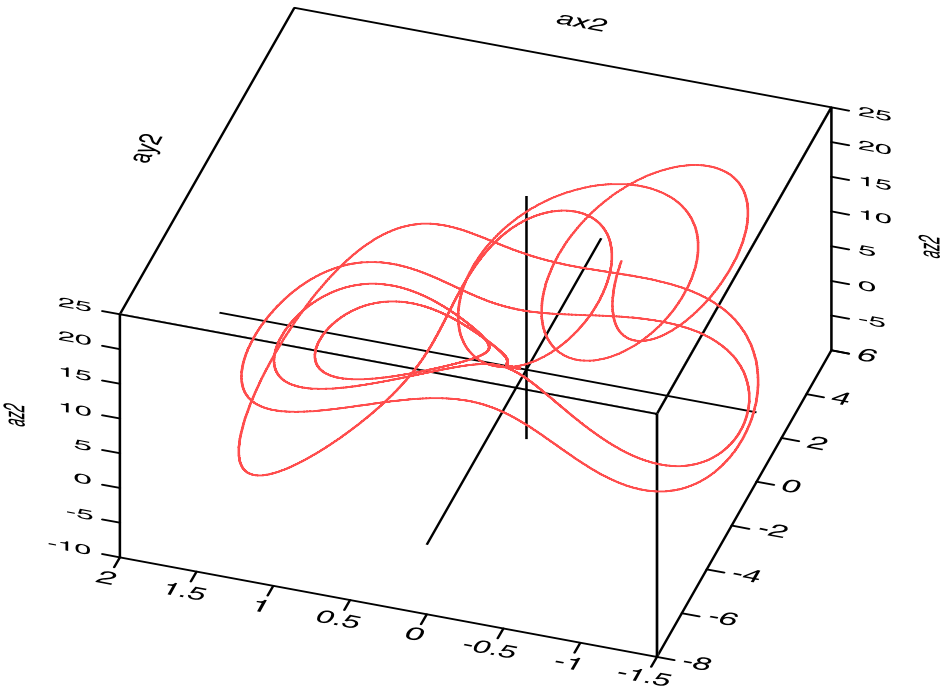

Figure 11 shows the $a_{x4} - a_{y4}$ phase plane results obtained from the output of the third receiver system. Figure 12 shows the $a_{z4} - a_{y4}$ phase plane results for this receiver. The processing of the input signal from the transmitter and the two previous receiver systems has resulted in a shifting of the orientation of the phase plane results for both sets of results from that indicated for the initial transmitter system.

Figure 11. This figure presents the phase plane, a_{x4} - a_{y4} for the output of the third receiver system. Parameters: $M_1 = 1.44$, $x = 0.08$, $z = 0.003$, $j = 16$ ($\eta = 3.00$).

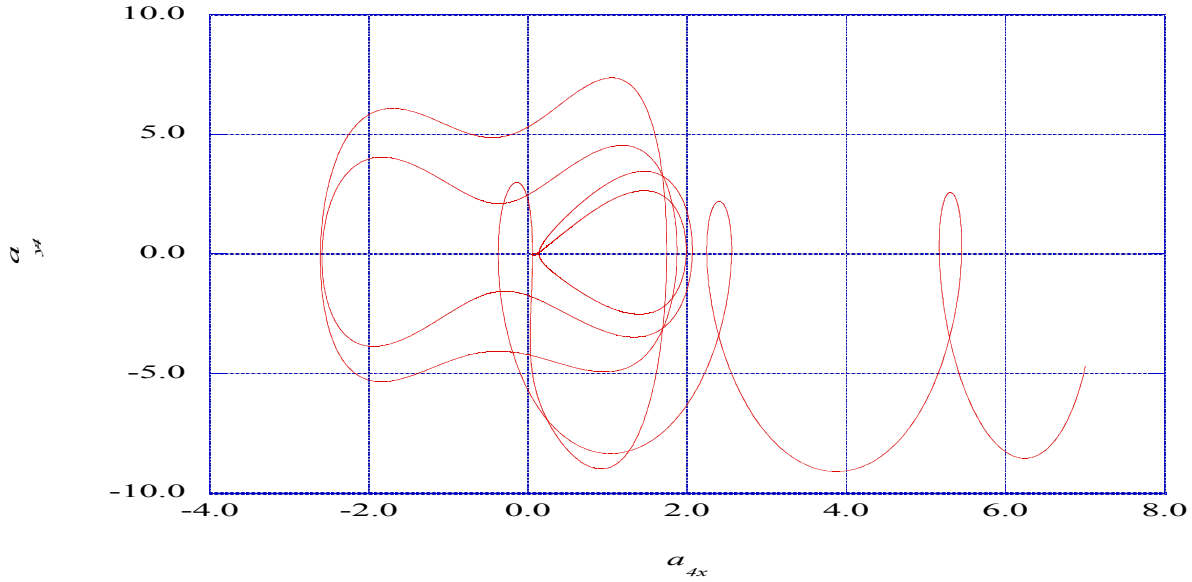

Figure 12. This figure presents the phase plane, $a_{z4} - a_{y4}$ for the output of the third receiver system. Parameters: $M_1 = 1.44$, $x = 0.08$, $z = 0.003$, $j = 16$ ($\eta = 3.00$).

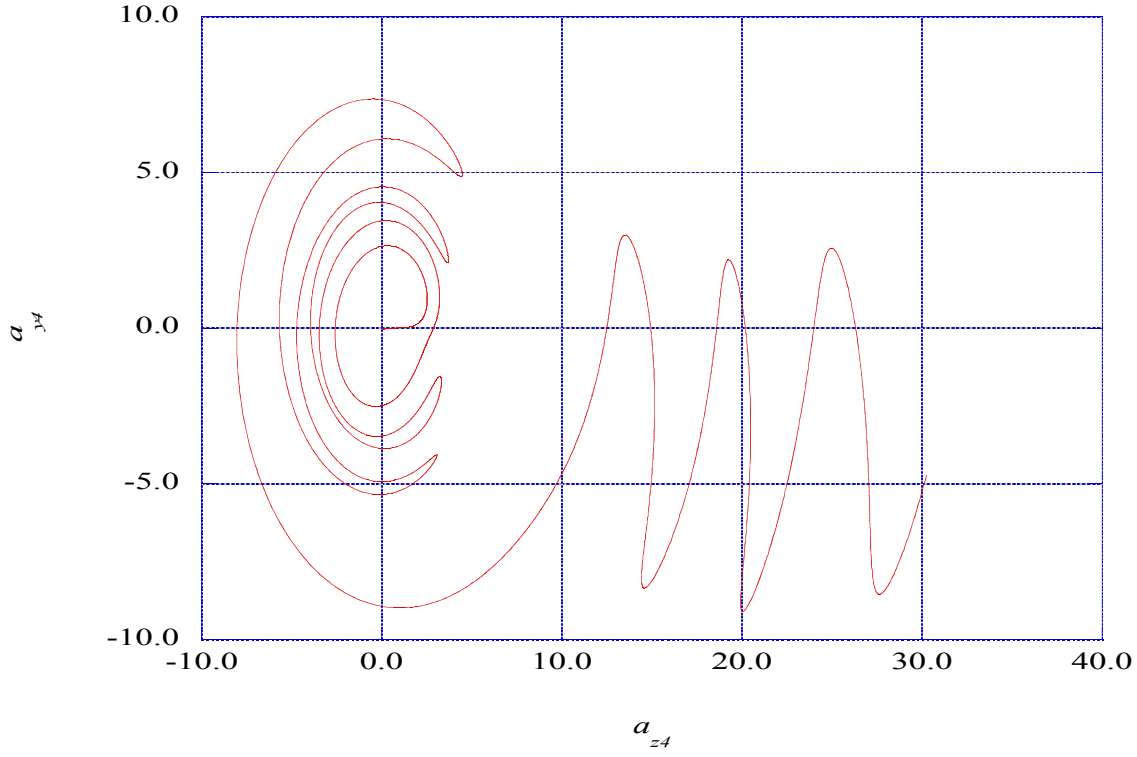

Figure 13 presents the three-dimensional plot of the output for the three velocity wave vectors from the third receiver. It is interesting to note that the first three receiver systems have transformed the fluctuating velocity wave vectors into a spiral configuration, and that the emergence of ordered regions in the a_x and a_y velocity wave vectors is apparent.

Figure 13. This figure presents a three-dimensional representation of the fluctuating velocity wave vector trajectories produced through the third receiver system. Parameters: $M_1 = 1.44$, $x = 0.08$, $z = 0.003$, $j = 16$ ($\eta = 3.00$).

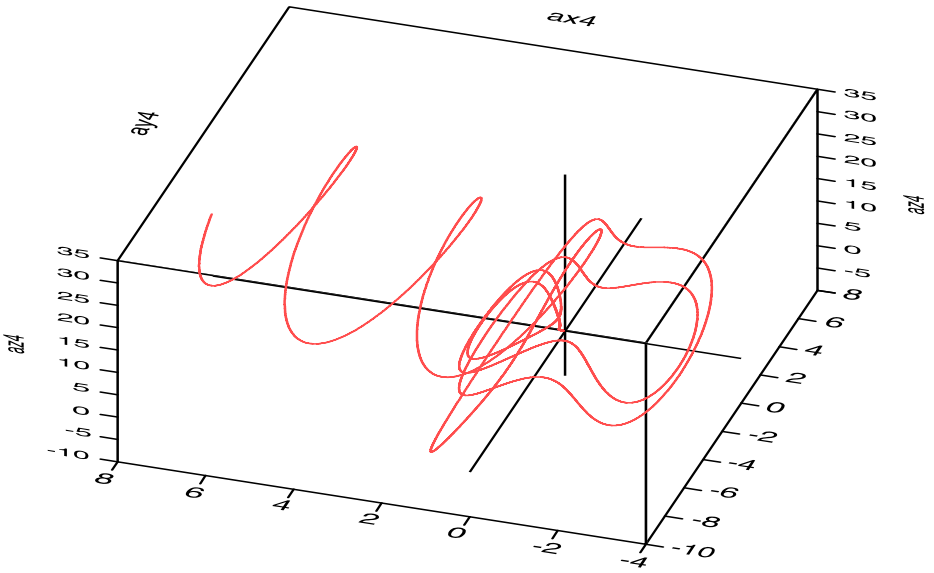

Figure 14 shows the $a_{x5} - a_{y5}$ phase plane results obtained from the output of the fourth receiver. Figure 15 shows the $a_{z5} - a_{y5}$ phase plane results for this receiver. The processing of the input signal from the transmitter plus the output signals from the previous receivers has resulted in the evolution of a directed spiral vortex form for the fluctuating velocity wave vectors.

Figure 14. This figure shows the phase plane, $a_{z5} - a_{y5}$ for the output of the fourth receiver system. Parameters: $M_1 = 1.44$, $x = 0.08$, $z = 0.003$, $j = 16$ ($\eta = 3.00$).

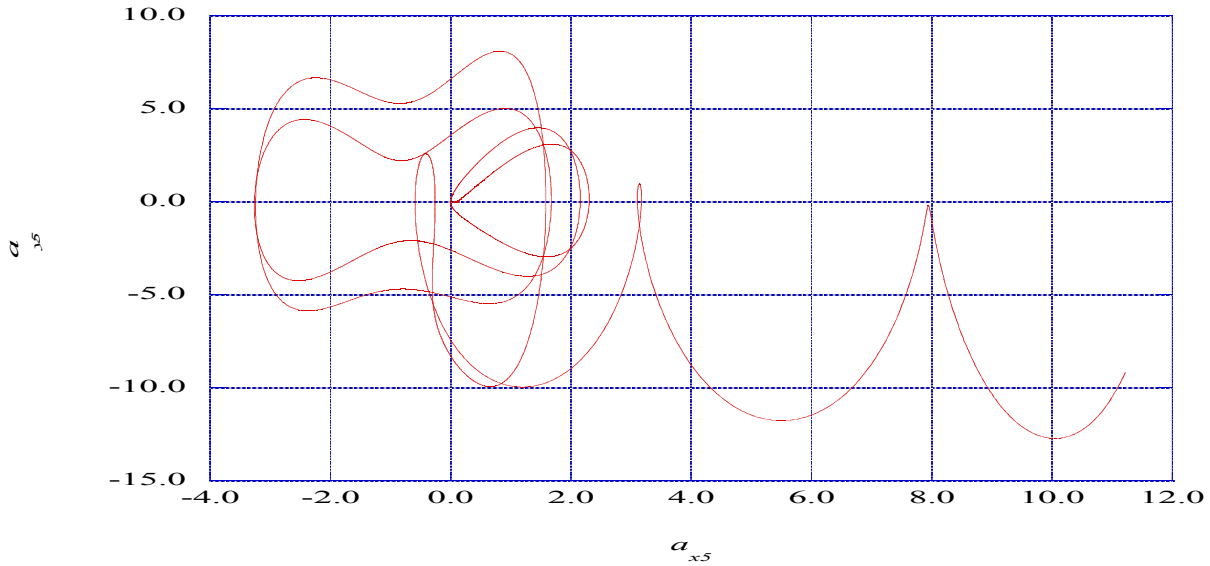

Figure 15. This figure presents the phase plane, $a_{z5} - a_{y5}$ for the output of the fourth receiver system. Parameters: $M_1 = 1.44$, $x = 0.08$, $z = 0.003$, $j = 16$ ($\eta = 3.00$).

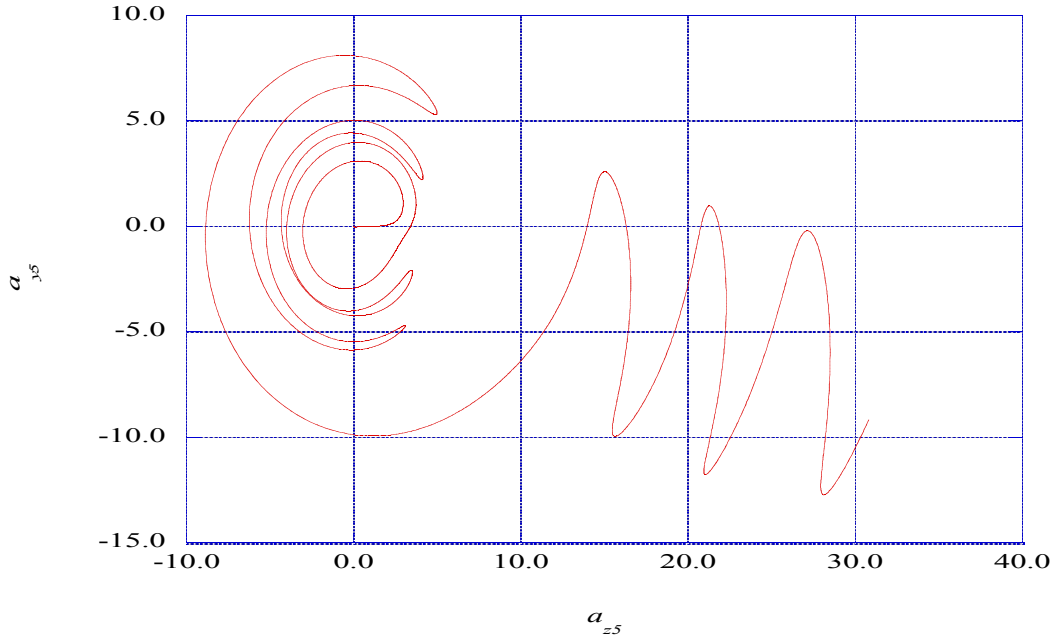

Figure 16 presents the three-dimensional plot of the output for the three velocity wave vectors from the fourth receiver. It is interesting to note that the fourth receiver has oriented the velocity wave vectors, and that the emergence of ordered regions in the a_{x5} and a_{y5} velocity wave vectors is apparent.

Figure 16. This figure presents a three-dimensional representation of the fluctuating velocity wave vector trajectories produced through the fourth receiver system. Parameters: $M_1 = 1.44$, $x = 0.08$, $z = 0.003$, $j = 16$ ($\eta = 3.00$).

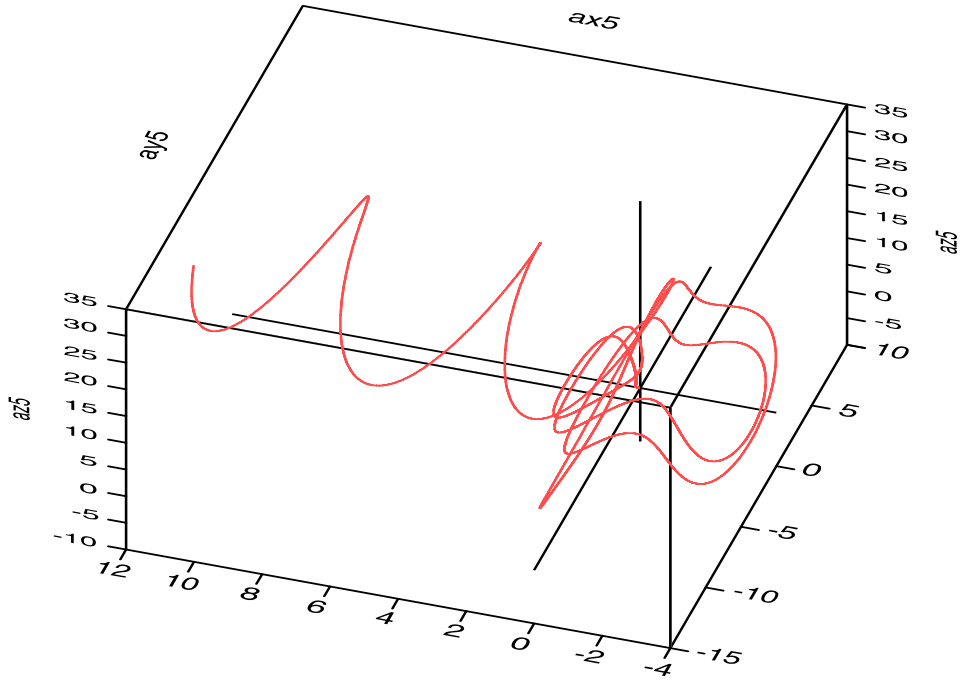

5.3. The Prediction of Spectral Entropy Rates from the Deterministic Results

The results from the time integration of the modified Townsend equations consist of nonlinear time series outputs for the composite wave number and for the three fluctuating velocity wave vectors. Chen [11] has presented a series of studies of methods for the extraction of structural information from time series information. In reference [12], a computer source code was presented which implemented the maximum entropy method (Burg's method) for spectral analysis of geophysical seismic time data records. This method considerably improves the spectral resolution for short records.

Burg's method has its theoretical roots in information theory (Cover and Thomas [31]), where a discussion and a proof of Burg's maximum entropy rate theorem are given. These authors also make reference to the work of Rissanen [32,33], where the maximum entropy method is related to the concept of Kolmogorov complexity [34].

One of the significant advantages of Burg's method is the enhancement of the spectral peaks in the power spectral density distribution. Our previous experience with Burg's method and the existence of useful source codes for the analysis of the predicted time series led to our use of this method for the evaluation of the power spectral density of the axial velocity wave vector, a_x, for each segment in the time series.

The method of computation used for the prediction of the distribution of the power spectral density rate is the method presented by Press *et al*. [35]. The power spectral density for the axial velocity wave vector time series is computed for 4,096 time step data samples from time step of 8,192 to time step 12,288. The selected time series is divided into 128 segments with 32 data sets per segment. Burg's method [35], is then applied to each segment of the 128 data sets to obtain 64 spiked values of the power spectral density of the axial velocity wave vector, f_r, for each particular segment.

The spectral entropy rate evaluated from the power spectral density is used as a measure of the degree of order within the nonlinear time series obtained from the solution of the modified Townsend equations for the fluctuating axial velocity wave vector.

The probability value for each particular power spectral density for a given time segment is first computed from $P_r = f_r \,/ \sum_r f_r$. The methods of Powell and Percival [13] and Grassberger and Procaccia [36] are then applied to the probability distributions for each time segment to develop the spectral entropy rate for the given segment. The spectral entropy rate (1/s) is then defined for the j-th time segment as:

$$s_j \_ spent = -\sum_r P_r \ln P_r \,. \tag{37}$$

The spectral entropy rate results for the transmitter system are presented in Figures 17. These spectral entropy rates are computed from 128 time data segments covering the block of nonlinear time series output from the time step of 8,192 to the time step of 12,288 at the vertical boundary-layer stations of j = 16 (η = 3.00) and for the span wise station nz = 4(z = 0.003) at the axial station of nx = 4 (x = 0.08). These results indicate a significant level of chaotic behavior of high spectral entropy rates (~0.35), interspersed with intermediate regions of lowered spectral entropy rates (~0.20). The important observation, however, is that several downward spikes of spectral entropy rates to zero value indicate the production of ordered structures within the axial velocity wave vector time series. Thus,

for the selected location in boundary-layer spatial coordinates, and for the particular values of weighting parameter and the initial conditions, the initial instability results for the transmitter system indicate a time-dependent transition process between ordered, partially ordered, and chaotic states.

Figure 17. The spectral entropy rate presented as a function of the segment number for the axial velocity wave vector, a_{x1} output from the initial transmitter system. Parameters: $M_1 = 1.44$, $x = 0.08$, $z = 0.003$, j = 16 ($\eta = 3.00$).

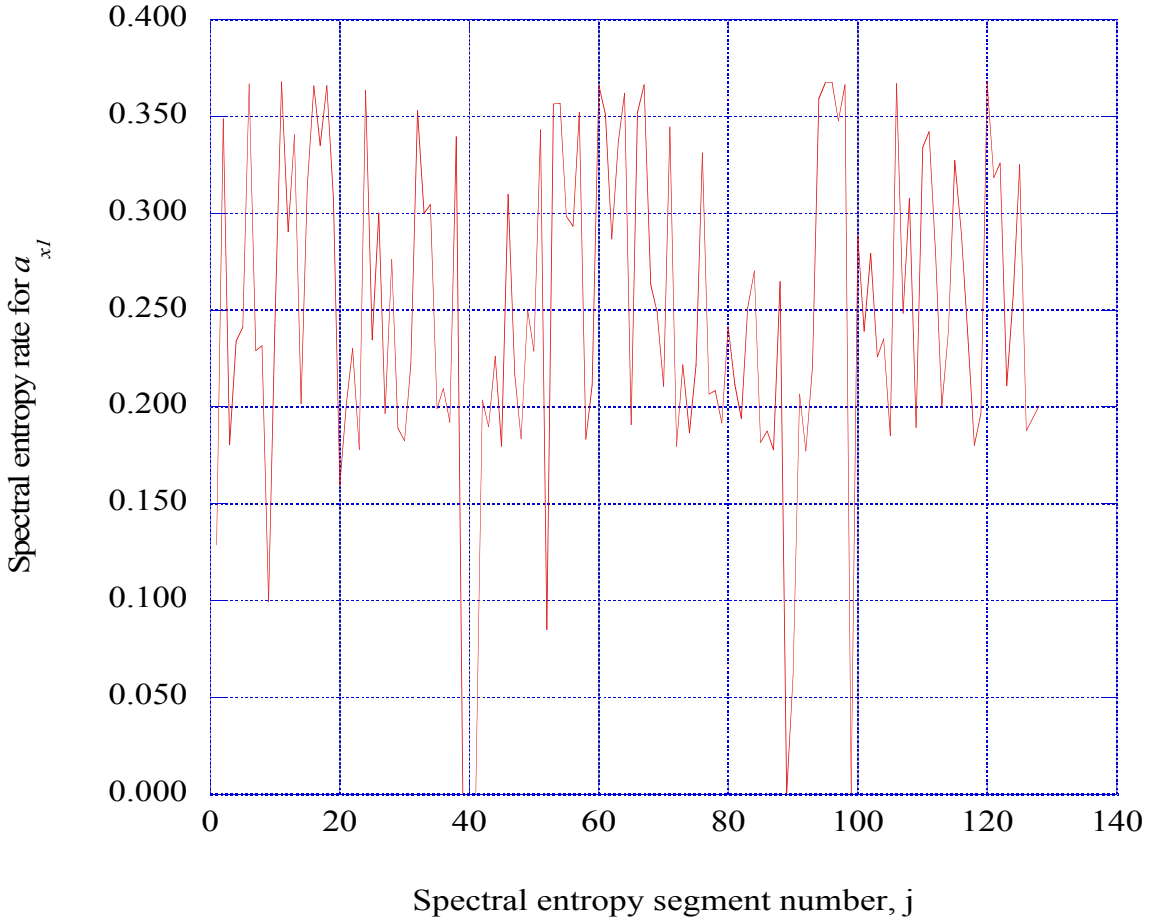

The spectral entropy rates for the signal from the third and fourth receiver systems are shown in Figures 18 and 19. These results also show a reduced rate of chaotic behavior, a region of partially ordered regions and more closely organized regions with low values of spectral entropy rate. These results indicate that the processing of the initial transmitter signal by the subsequent receiver systems has recovered additional regions of ordered signals. It should be noted that the processing by additional receiver systems does not converge to a well-ordered state. The addition of a fifth receiver system produces a complete disruption of the ordering process.

Figure 19 shows the results for the spectral entropy rate analysis of the output signal from the fourth receiver system. The number of segments with zero production of spectral entropy has doubled over the output signal from the previous receiver.

Figure 18. The spectral entropy rate is shown as a function of the segment number for the axial velocity wave vector, a_{x4} output from the third receiver system system. Parameters: $M_1 = 1.44$, $x = 0.08$, $z = 0.003$, j = 16 ($\eta = 3.00$).

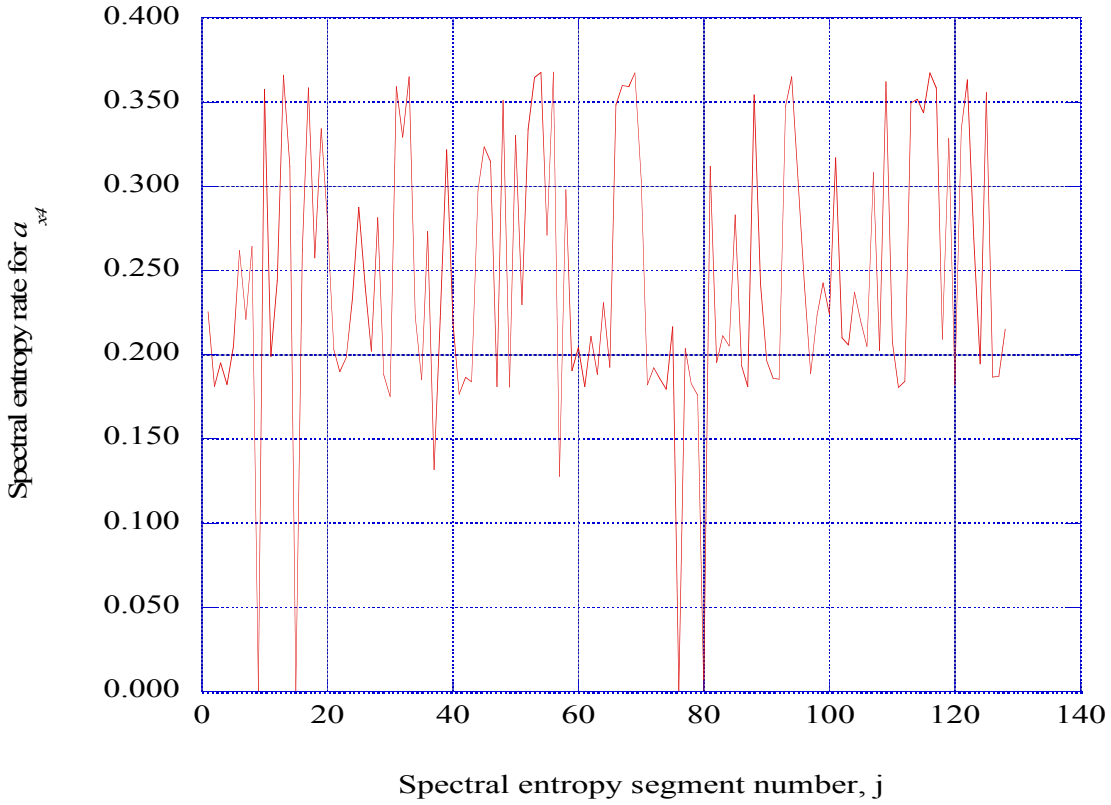

Figure 19. The spectral entropy rate presented as a function of the segment number for the axial velocity wave vector, a_{x5} output from the fourth receiver system. Parameters: $M_1 = 1.44$, $x = 0.08$, $z = 0.003$, j = 16 ($\eta = 3.00$).

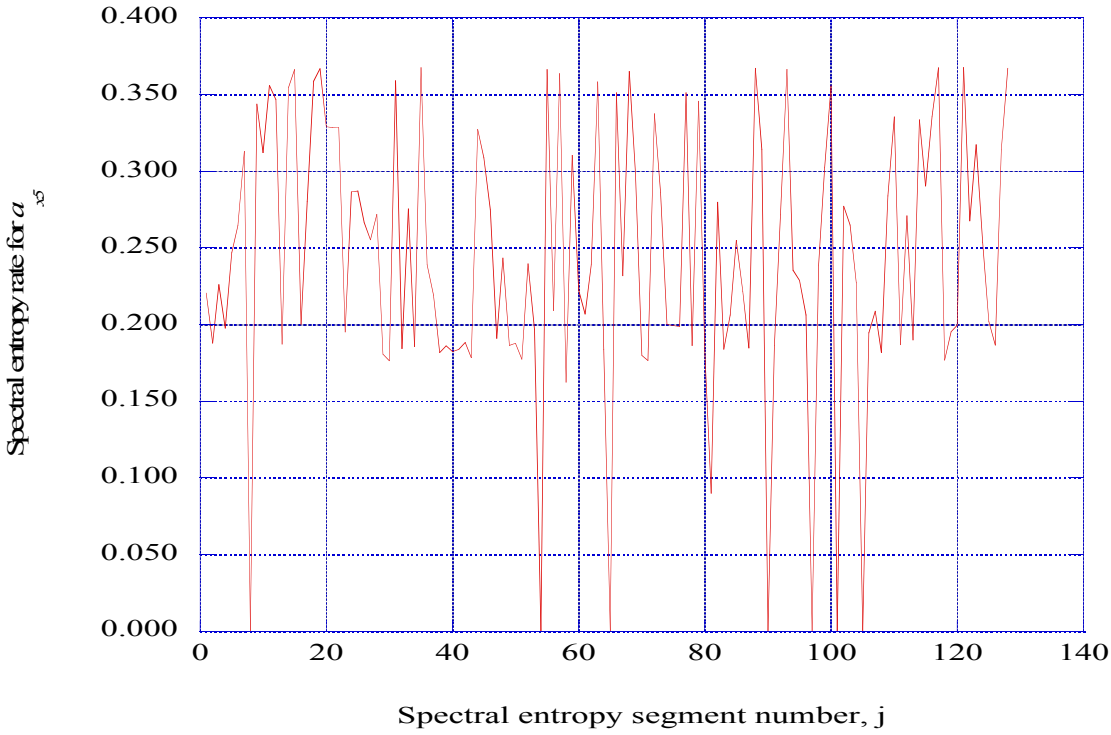

6. Discussion

The basic consideration for the selection of the flight regime of a flight Mach number of 1.44 at an altitude of approximately 21.3 km is that the normal shock wave at these conditions produces the thermodynamic and transport properties in the subsonic flow over a flat plate surface that produces the prediction of the development of downstream boundary layer instabilities.

Evaluation of the thermodynamic and thermal transport properties has been carefully implemented to provide an accurate basis for the evaluation of the time-dependent stability characteristics of the three-dimensional boundary-layer structure. The boundary-layer velocity profiles for the x-y and z-y have been determined using the methods of Cebeci and Bradshaw [6]. The x-z plane flat boundary-layer surface is raised to an elevation in the y-direction that provides the appropriate z-y plane velocity gradients in line with the corresponding x-y plane velocity gradients.

The Townsend equations are Fourier transformed into a set of six simultaneous, nonlinear differential equations for the set of wave number vectors and the velocity wave vectors. To accomplish the separation of the set of wave number equations from the set of velocity wave vector equations, the transfer matrix operator is replaced by a heuristically determined coupling coefficient that includes a small weighting factor and a periodic function of the time-dependent axial wave number magnitude.

The solutions for the wave number vectors and the various velocity wave vectors indicate an initial delay period during which no changes are indicated. Then the wave number solutions indicate an aperiodic oscillatory behavior.

The oscillatory behavior of the wave number vector components is transmitted to the solutions for the velocity wave vectors indicating an initial periodic behavior and then a more chaotic behavior. Typical behaviors of this region of the velocity wave vector solutions for a flight Mach number of 1.44 are represented in Figures 5, 6 and 7.

The power spectral density of the axial velocity wave vector over the time domain of the aperiodic oscillator behavior is obtained by Burg's method. This method is an accurate tool for the extraction of appropriate spectral characteristic from a given time series of data. The method of spectral entropy rate analysis is applied to the power spectral density time series to extract information about the characteristics of the resulting axial velocity wave vector time series. We consider the spectral entropy rate value of approximately 0.35 as indicating a nearly chaotic behavior, while a considerable portion of the time-dependent behavior of the axial velocity wave vector is in a partially ordered structural state, with spectral entropy rate values of approximately 0.20. Figure 17 also shows results that ordered structures, with essentially zero spectral entropy production, are produced within the three-dimensional boundary-layer flow system.

The axial velocity wave vector signal output from the initial Lorenz-type transmitter system is sent as input to the second unit, an in place identical Lorenz-type receiver system. The input signal to the third unit, a second identical Lorenz-type receiver system, is made up of the sum of the transmitter output signal and the output signal of the first receiver system. Four receiver systems are including in the processing of the chaotic-masked output signal from the original transmitter system. Figures 18 and 19 indicate that the receiver processing of the chaotic-masked output signal from the original transmitter system has extracted information representing ordered regions of an axially directed spiral vortex form. It should be noted that the inclusion of additional receiver systems does not indicate a

converging behavior for the receiver output signals. The inclusion of a fifth receiver system indicates an output much larger in magnitude with the axial velocity wave vector in the negative axial direction. The detailed behavior of the receiver systems in the chaotic synchronization of the masked signals is presently not understood, perhaps providing an interesting area of research.

We find that in a small subdomain of the time integration process prior to the onset of unbounded solutions, oscillatory fluctuations are predicted in both the wave number time series solutions and in the time series solutions for the three fluctuating velocity wave vectors. These oscillatory solutions are found for the boundary-layer vertical stations of j = 16 (η = 3.00) in the x-y plane and j = 16 (η = 3.00) in the z-y plane for the Mach number of 1.44 at the altitude of 21.3 km. Considering that the solutions represent the initiation of oscillatory behavior due to nonlinear interactions at the beginning of the process and that the time subdomain is short within the time integration process prior to the onset of unbounded solutions, the indication of the nonlinear generation of ordered structures may very well represent the actual physical generation of such structures within this type of laminar boundary-layer flow.

7. Conclusions

The complete set of equations for the fluctuating velocity wave vectors within a boundary-layer flow has been reduced to a set of equations similar to the Lorenz equations with the introduction of the velocity gradients for specified vertical boundary-layer stations in both the x-y and z-y planes, the y location for the z-y plane velocity gradients and an internal feedback weighting parameter factor *K* in the modified Townsend equations. The computational technique has been applied to the subsonic flat plate boundary layer downstream of a normal shock wave for a flight Mach number of 1.44 at an altitude of approximately 21.3 km. The computational results indicate that for the three-dimensional configuration considered, partially ordered and fully ordered structures are generated within the boundary layer by internal nonlinear interactions. The measure for the characterization of the computed structures is the spectral entropy rate calculated from the power spectral density properties of the nonlinear time series output of the deterministic equations. The spectral entropy rate results show time-dependent transitions from chaotic to partially ordered motion, then back to chaotic motion, in a repetitive manner within the chaotic-masked nonlinear time-series output. Fully ordered regions are extracted from the deterministic nonlinear time series signal from the transmitter system with successive processing by identical Lorenz-type receiver systems. These receiver systems have extracted results that indicate that ordered regions may occur that may be representative of an axially directed spiral vortex form produced by nonlinear interactions within the boundary-layer system.

References

1. Berlin, S.; Henningson, D.S. A nonlinear mechanism for receptivity of free-stream disturbances. *Phys. Fluids* **1999**, *11*, 3749–3760.
2. Hoepffner, J.; Brandt, L. Stochastic approach to the receptivity problem applied to bypass transition in boundary layers. *Phys. Fluids* **2008**, *20*, 024108:1–024108:4.
3. Waleffe, F. Homotopy of exact coherent structures in plane shear flows. *Phys. Fluids* **2003**, *15*, 1517–1534.

4. Cherubini, S.; De Palma, P.; Robinet, J.-C.; Bottaro, A. Edge states in a boundary layer. *Phys. Fluids* **2011**, 23, 051750:1–051750:4.
5. Duguet, Y.; Schlatter, P.; Henningson, D.S. Localized edge states in plane Couette flow. *Phys. Fluids* **2009**, *21*, 111701:1–111701:5.
6. Cebeci, T.; Bradshaw, P. *Momentum Transfer in Boundary Layers*; Hemisphere: Washington, DC, USA, 1977.
7. Hansen, A.G. *Similarity Analyses of Boundary Value Problems in Engineering*; Prentice-Hall, Inc.: Englewood Cliffs, NJ, USA, 1964; pp. 86–92.
8. Townsend, A.A. *The Structure of Turbulent Shear Flow*, 2nd ed.; Cambridge University Press: Cambridge, UK, 1976, pp. 45–49.
9. Isaacson, L.K. Spectral Entropy in a Boundary-Layer Flow. *Entropy* **2011**, *13*, 402–421.
10. Isaacson, L.K. Control Parameters for Boundary-Layer Instabilities in Unsteady Shock Interactions. *Entropy* **2012**, *14*, 131–160.
11. Chen, C.H. *Digital Waveform Processing and Recognition*; CRC Press, Inc.: Boca Raton, FL, USA, 1982; pp. 131–158.
12. Press, W.; Teukolsky, S.A.; Vetterling, W.T.; Flannery, B.P. *Numerical Recipes in C: The Art of Scientific Computing*, 2nd ed.; Cambridge University Press: Cambridge, UK, 1992; pp. 572–575.
13. Powell, G.E.; Percival, I.C. A spectral entropy method for distinguishing regular and irregular motions for Hamiltonian systems. *J. Phys. Math. Gen*. **1979**, *12*, 2053–2071.
14. Pecora, L.M.; Carroll, T.L. Synchronization in chaotic systems. In *Controlling Chaos: Theoretical and Practical Methods in Non-linear Dynamics*; Kapitaniak, T., Ed.; Academic Press Inc.: San Diego, CA, USA, 1996; pp. 142–145.
15. Pérez, G.; Cerdeiral, H.A. Extracting messages masked by chaos. In *Controlling Chaos: Theoretical and Practical Methods in Non-linear Dynamics;* Kapitaniak, T., Ed.; Academic Press Inc.: San Diego, CA, USA, 1996; pp. 157–160.
16. Cuomo, K.M.; Oppenheim, A.V. Circuit implementation of synchronized chaos with applications to communications. In *Controlling Chaos: Theoretical and Practical Methods in Non-linear Dynamics*; Kapitaniak, T., Ed.; Academic Press Inc.: San Diego, CA, USA, 1996; pp. 153–156.
17. Feng, J.C.; Tse, C.K. *Reconstruction of Chaotic Signals with Applications to Chaos-Based Communications*; World Scientific Publishing Co. Pte. Ltd.: Hackensack, NJ, USA, 2008; pp. 165–213.
18. Zucrow, M.J.; Hoffman, J.D. *Gas Dynamics: Vol. I*; John Wiley & Sons, Inc.: New York, NY, USA, 1976; pp. 335–349.
19. Sonntag, R.E.; Van Wylen, G.J. *Fundamentals of Statistical Thermodynamics*; Robert Krieger Publishing Company, Inc.: Malabar, FL, USA, 1985.
20. McBride, B.J.; Gordon, S.; Reno, M.A. *Coefficients for Calculating Thermodynamic and Transport Properties of Individual Species*; NASA TM 4513, National Aeronautics and Space Administration: Washington, DC, USA, October 1993.
21. Dorrance, W.H. *Viscous Hypersonic Flow*; McGraw-Hill Book Company, Inc.: New York, NY, USA, 1962; pp. 276–315.
22. Zucrow, M.J.; Hoffman, J.D. *Gas Dynamics: Vol. I*; John Wiley & Sons, Inc.: New York, NY, USA, 1976; pp. 708–709.

23. Anderson, J.D., Jr.; *Hypersonic and High-Temperature Gas Dynamic*, 2nd ed.; American Institute of Aeronautics and Astronautics, Inc.: Reston, VA, USA, 2006; p. 616.
24. Sagaut, P.; Cambon, C. *Homogeneous Turbulence Dynamics*; Cambridge University Press: New York, NY, USA, 2008.
25. Mathieu, J.; Scott, J. *An Introduction to Turbulent Flow*; Cambridge University Press: New York, NY 10011-4211, USA, 2000, pp. 251–261.
26. Landau, L.D.; Lifshitz, E.M. *Quantum Mechanics: Non-Relativistic Theory*; Addison-Wesley Publishing Company, Inc.: Reading MA, USA, 1958; pp. 143–144.
27. Pyragas, K. Continuous control of chaos by self-controlling feedback. In *Controlling Chaos: Theoretical and Practical Methods in Non-linear Dynamics*; Kapitaniak, T., Ed.; Academic Press Inc.: San Diego, CA, USA, 1996; pp. 118–123.
28. Hellberg, C.S.; Orszag, S.A. Chaotic behavior of interacting elliptical instability modes. *Phys. Fluids* **1988**, *31*, 6–8.
29. Isaacson, L. K. Deterministic Prediction of the Entropy Increase in a Sudden Expansion. *Entropy* **2011**, *13*, 402–421.
30. Press, W.; Teukolsky, S.A.; Vetterling, W.T.; Flannery, B.P. *Numerical Recipes in C: The Art of Scientific Computing*, 2nd ed.; Cambridge University Press: Cambridge, UK, 1992; pp. 710–714.
31. Cover, T.M.; Thomas, J.A. *Elements of Information Theory*, 2nd ed.; John Wiley & Sons, Inc.: Hoboken, NJ, USA, 2006; pp. 415–421.
32. Rissanen, J. Complexity and Information in Data. In *Entropy*; Greven, A., Keller, G., Warnecke, G., Eds.; Princeton University Press: Princeton, NJ, USA, 2003; pp. 299–327.
33. Rissanen, J. *Information and Complexity in Statistical Modeling;* Springer Science+Business Media, LLC: New York, NY, USA, 2007.
34. Li, M.; Vitányi, P. *An Introduction to Kolmogorov Complexity and Its Applications;* Springer Science+Business Media, LLC: New York, NY, USA, 2008.
35. Press, W.; Teukolsky, S.A.; Vetterling, W.T.; Flannery, B.P. *Numerical Recipes in C: The Art of Scientific Computing*, 2nd ed.; Cambridge University Press: Cambridge, UK, 1992; pp. 572–575.
36. Grassberger, P.; Procaccia, I. Estimation of the Kolmogorov entropy from a chaotic signal. *Phys. Rev. A* **1983**, *28*, 2591–2593.